Electronic Supplementary Material – Hydrogeology Journal

Enhancing geological and hydrogeological understanding of the Precipice Sandstone aquifer of the Surat Basin, Great Artesian Basin, Australia, through model inversion of managed aquifer recharge datasets

Phil Hayes[1*], Chris Nicol, Andrew D. La Croix, Julie Pearce, Sebastian Gonzalez, Jiahao Wang, Ahmed Harfoush, Jianhua He, Andrew Moser, Lauren Helm, Ryan Morris, David Gornall

[1]Centre for Natural Gas, University of Queensland, Brisbane, Australia 4072
*corresponding author: Phil Hayes (Phil.hayes@uq.edu.au)

Electronic supplementary material consists of:

- Conversions between groundwater and reservoir engineering units
- Figures showing plots of observation well and modelled responses to MAR injection. Note the location of all wells is provided on Figure 8 of the main article.
- Two hydrographs showing null responses at Emu Park and Armidale monitoring bores.

Conversions between groundwater and reservoir engineering units

The applied conversion methods for permeability and storage estimates in reservoir engineering units are summarised as follows:

Intrinsic permeability (k, in milli-Darcy [mD]) was derived from hydraulic conductivity (K_x [m/day]) as follows:

$$k = K_x \frac{\mu}{\rho g \times 9.869^{-16} \times 86400}$$

where ρ=water density [kg/m^3] (assumed uniform 987), g=acceleration due to gravity [m/sec^2] (assumed uniform 9.81), μ=fluid viscosity [Pa.sec].

Fluid viscosity, μ, was estimated as varying with formation depth and temperature based on the local geothermal gradient, using the Vogel–Fulcher–Tammann–Hesse equation (Fulcher 1925; Vogel 1925; Tammann and Hesse 1926):

$$\mu = e^{A+\frac{B}{C+T}}$$

Where: A (-3.7188), B (578.919) and C (-137.546) are fitted exponent parameters for water, and T is the water temperature in degrees Kelvin.

Temperature at 0 m datum was estimated at 29.36˚C, with a thermal gradient of 0.0207 ˚C/m. Formation depth was taken as the midpoint of the Precipice Sandstone.

Fluid density variation over the temperature range is a second order effect compared to viscosity variation with temperature, and was ignored.

Compressibility (β [/Pa]) was derived from specific storage (Ss [/m]) as follows:

$$(\beta_{\text{rock}} + \beta_{\text{water}}) = \frac{\text{Ss}}{\text{ratio}_{\text{net}_{\text{to}_{\text{gross}}}} \rho g \phi}$$

where: Ss=specific storage [/m]; Φ=aquifer porosity [-] (assumed constant 0.2); $\text{ratio}_{\text{net\_to\_gross}}$= Net to Gross ratio (assumed constant 1.0); β_{rock}=rock compressibility [/Pa]; and β_{water} =water compressibility [/Pa].

Density and gravity were assumed constant as per the intrinsic permeability conversion discussed above.

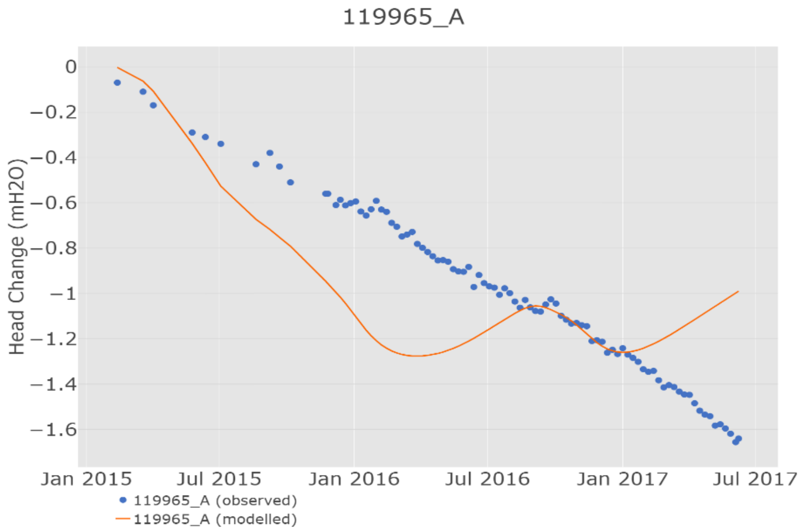

Figure S1 Modelled and observed change in groundwater level at well 119965_A

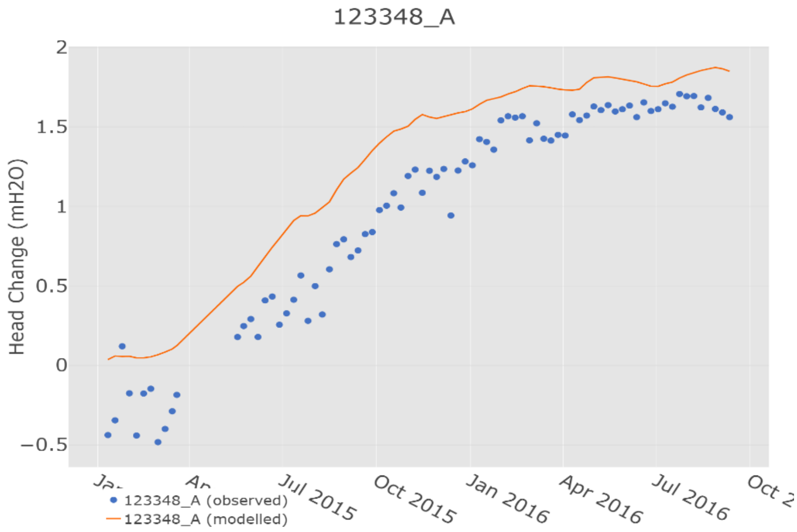

Figure S2 Modelled and observed change in groundwater level at well 123348_A

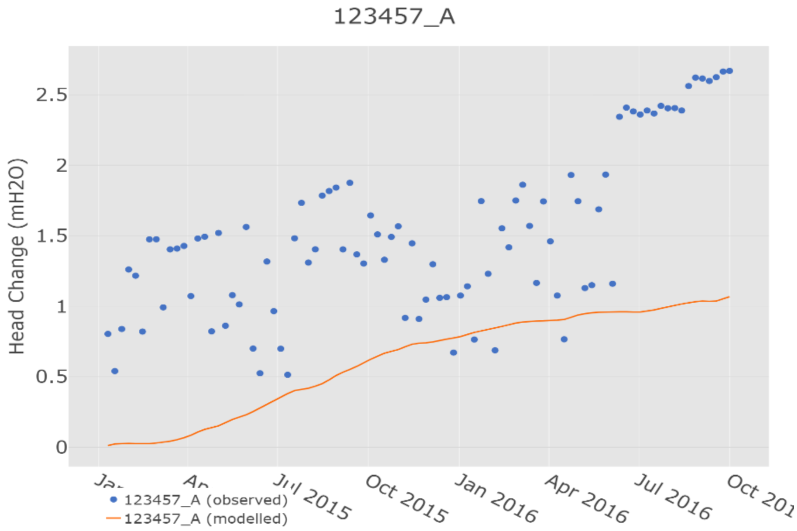

Figure S3 Modelled and observed change in groundwater level at well 123457_A

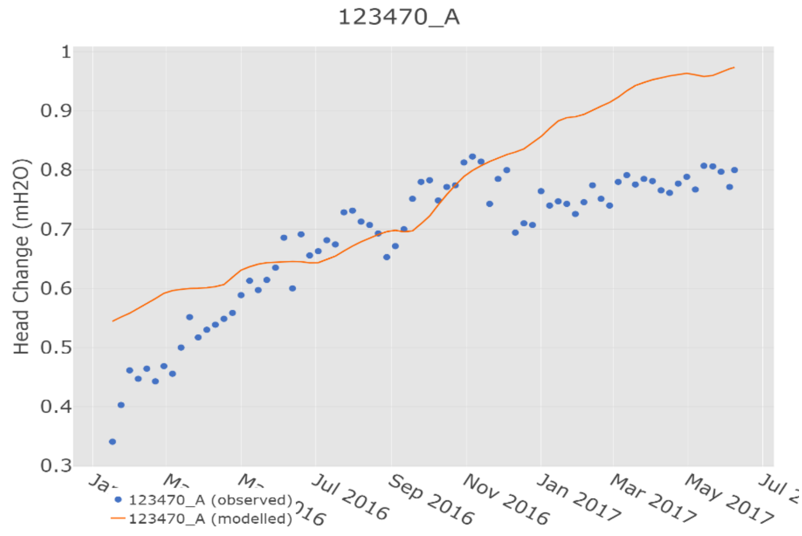

Figure S4 Modelled and observed change in groundwater level at well 123470_A

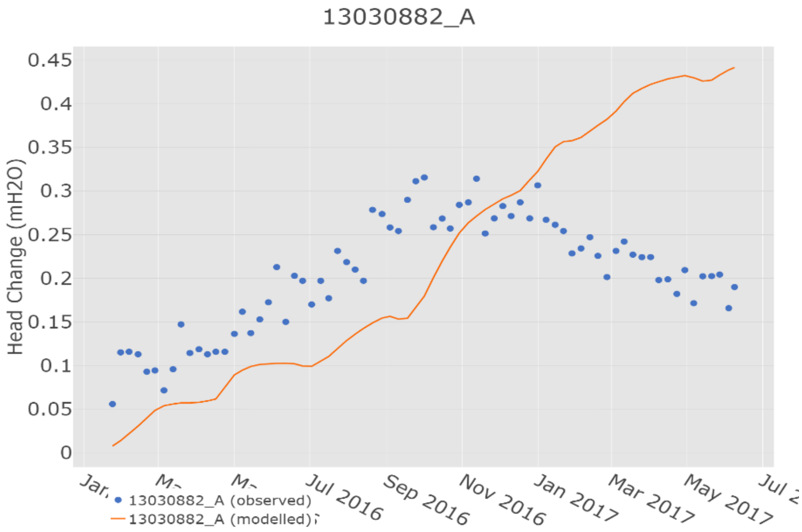

Figure S5 Modelled and observed change in groundwater level at well 13030882_A

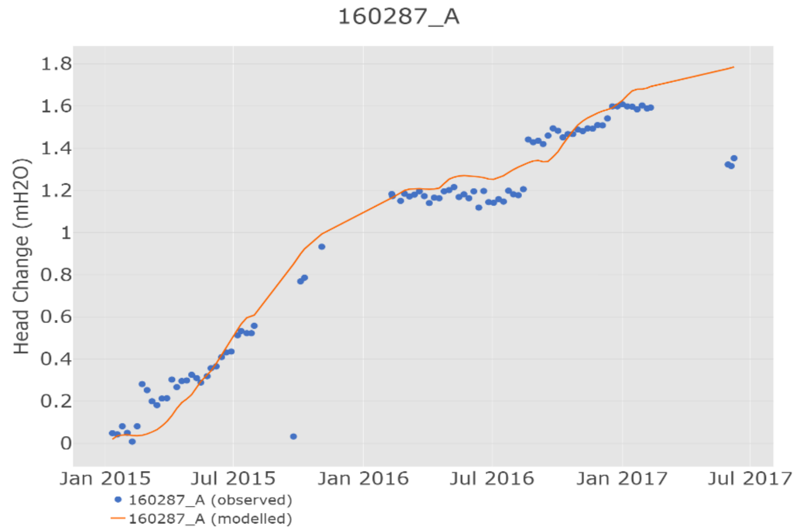

Figure S6 Modelled and observed change in groundwater level at well 160287_A

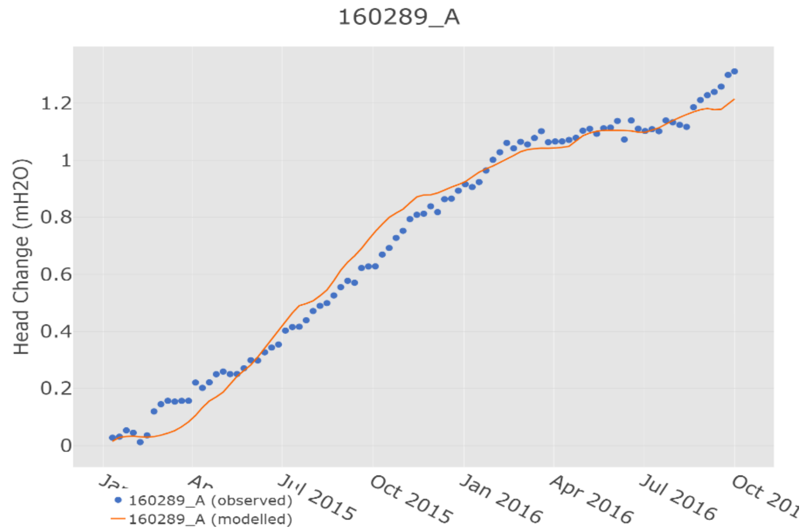

Figure S7 Modelled and observed change in groundwater level at well 160289_A

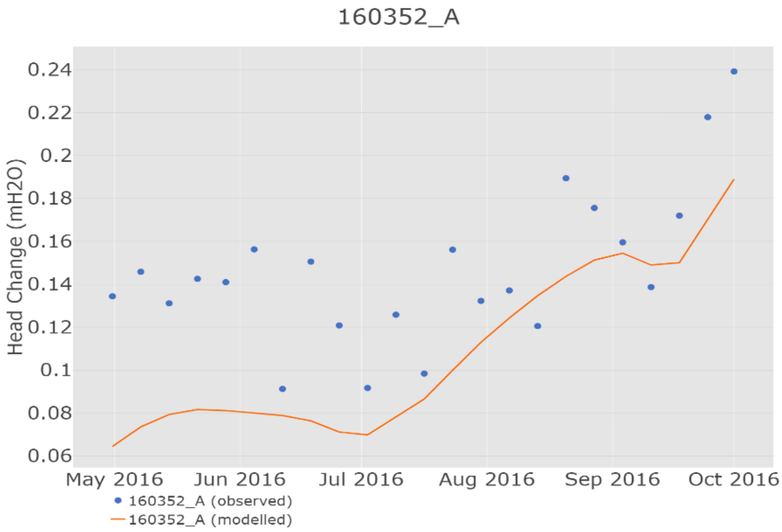

Figure S8 Modelled and observed change in groundwater level at well 160352_A

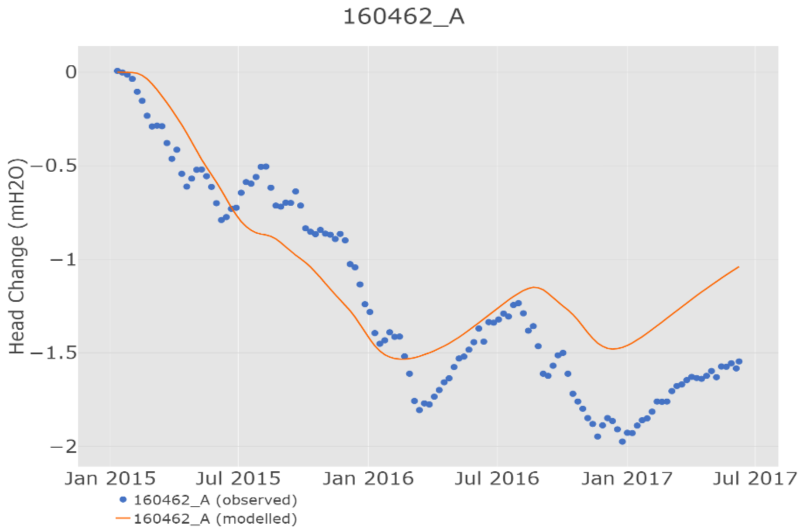

Figure S9 Modelled and observed change in groundwater level at well 160462_A

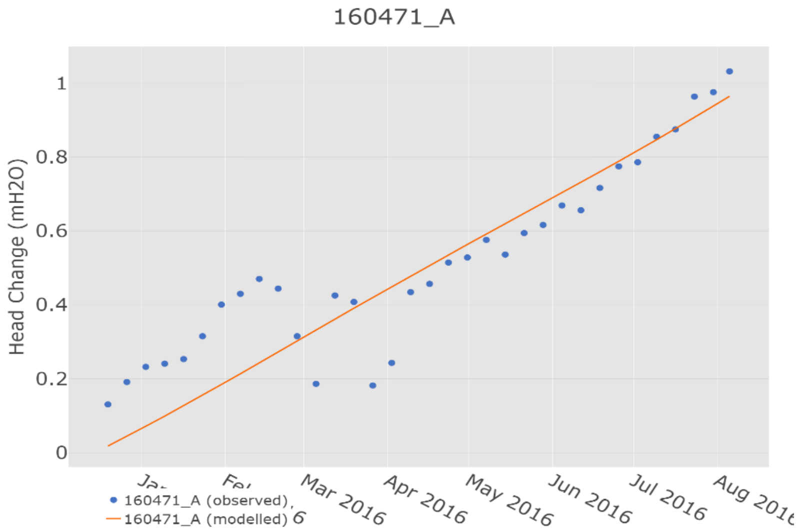

Figure S10 Modelled and observed change in groundwater level at well 160471_A

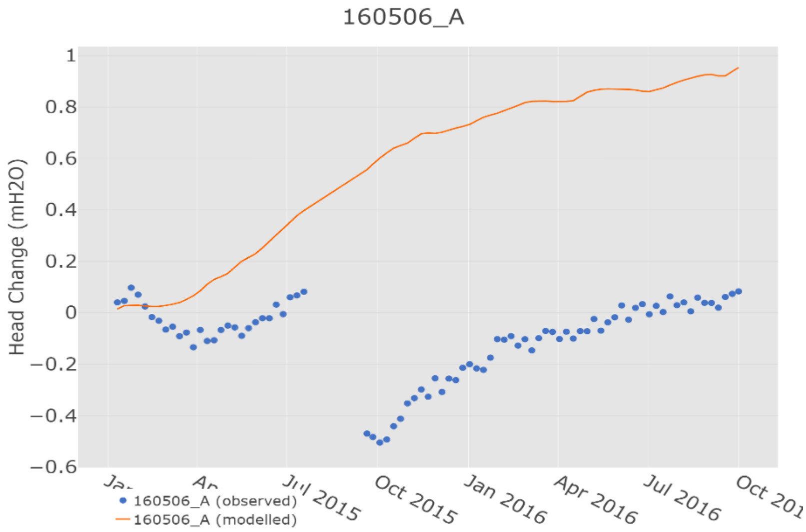

Figure S11 Modelled and observed change in groundwater level at well 160506_A

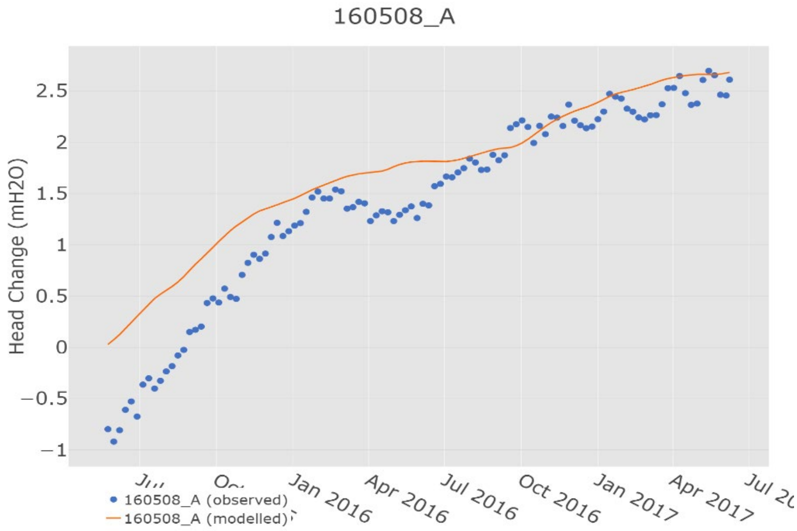

Figure S12 Modelled and observed change in groundwater level at well 160508_A

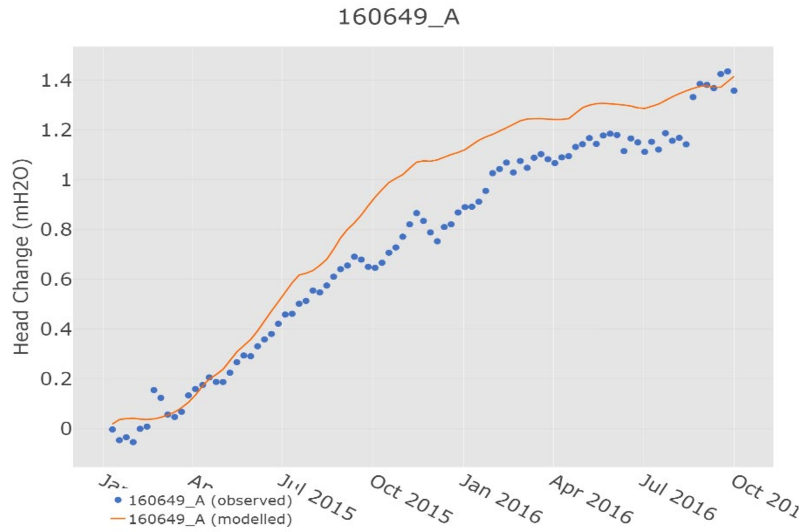

Figure S13 Modelled and observed change in groundwater level at well 160649_A

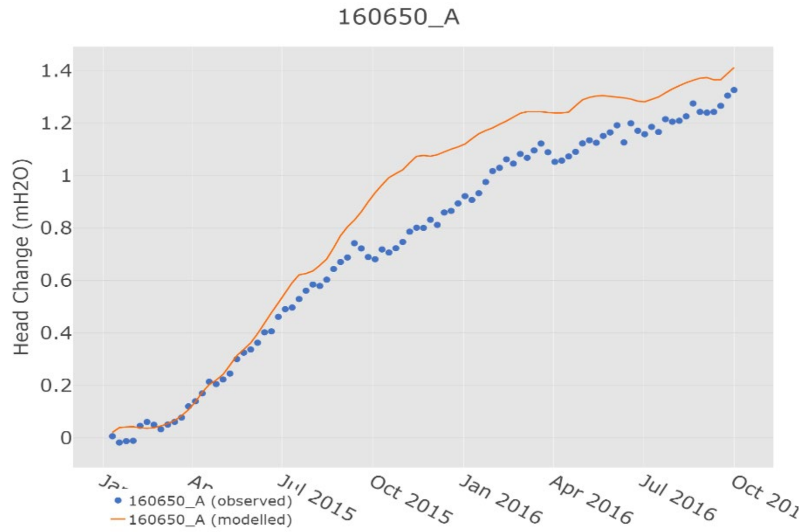

Figure S14 Modelled and observed change in groundwater level at well 160650_A

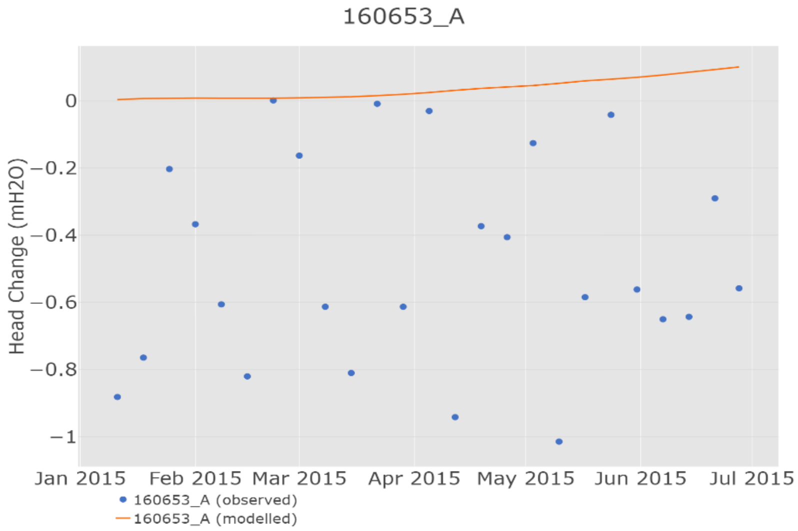

Figure S15 Modelled and observed change in groundwater level at well 160653_A

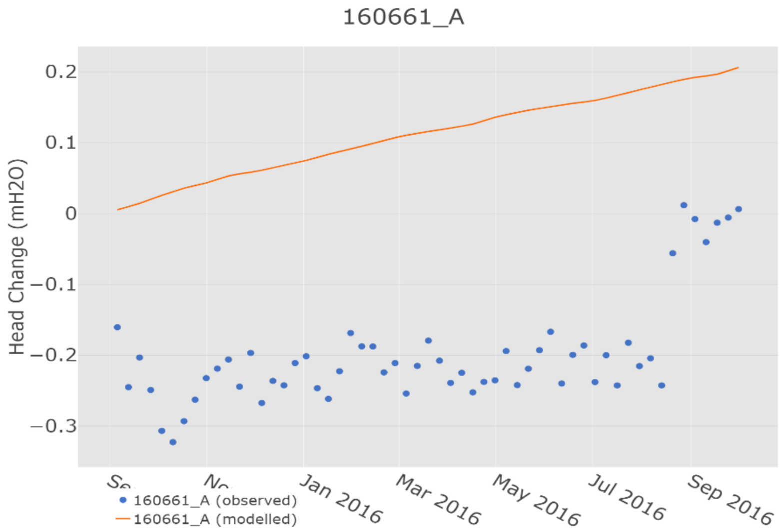

Figure S16 Modelled and observed change in groundwater level at well 160661_A

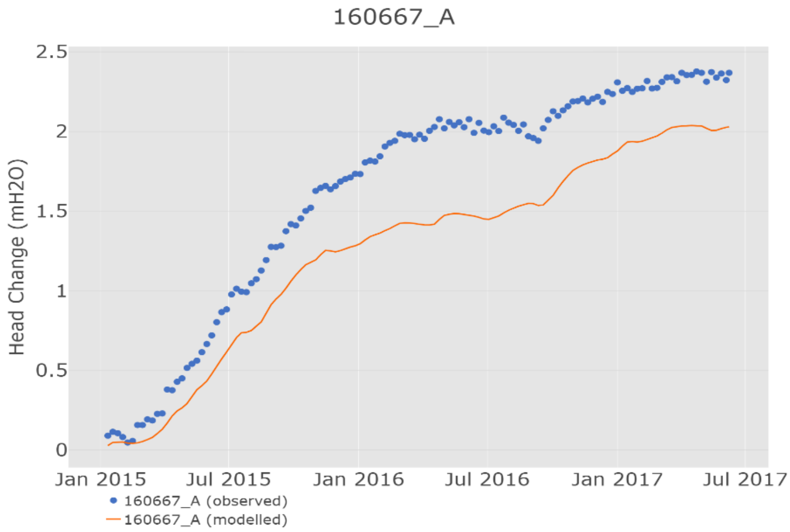

Figure S17 Modelled and observed change in groundwater level at well 160667_A

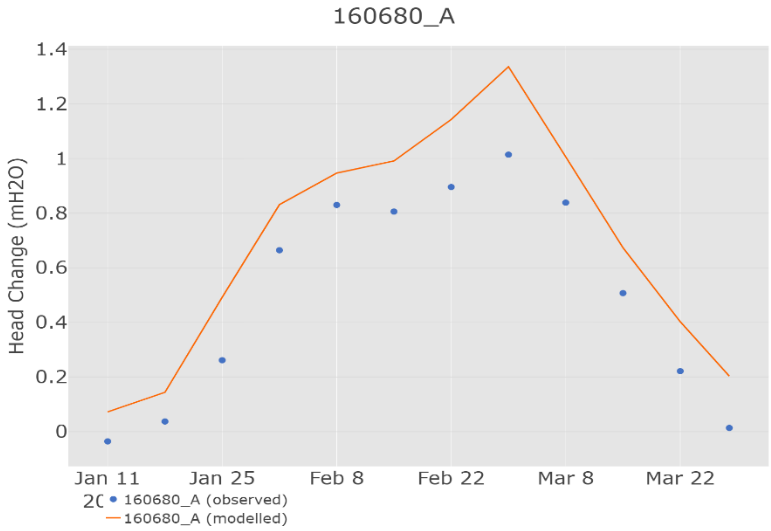

Figure S18 Modelled and observed change in groundwater level at well 160680_A

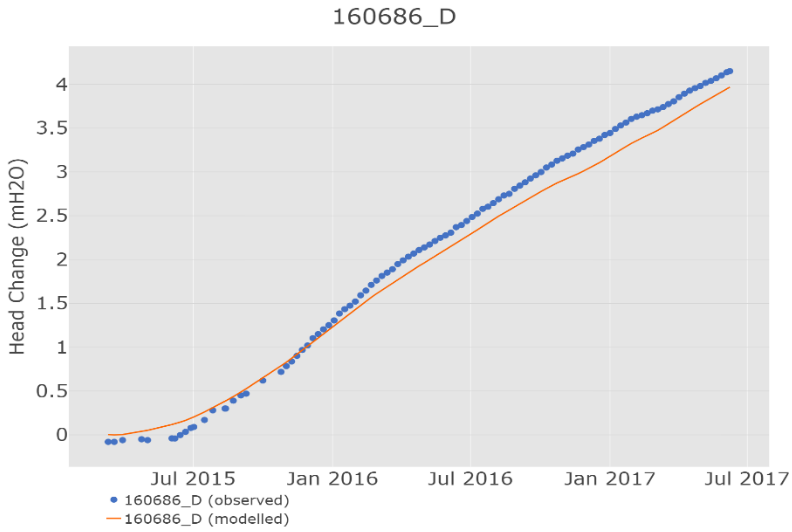

Figure S19 Modelled and observed change in groundwater level at well 160686_D

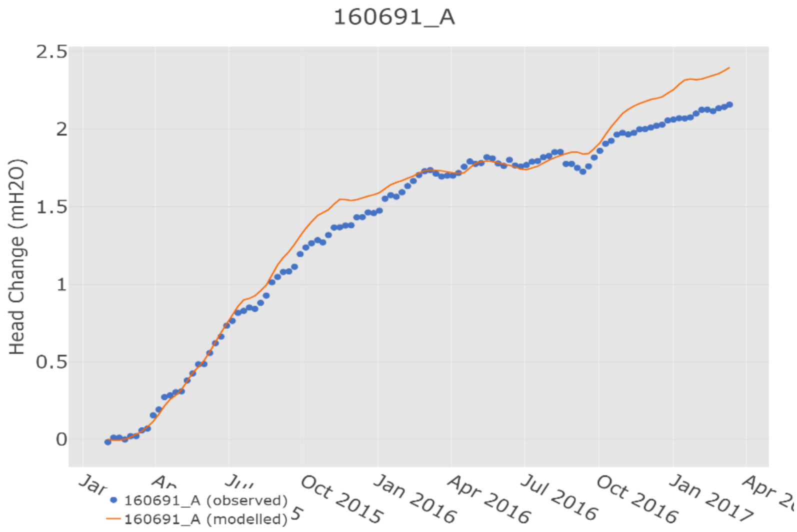

Figure S20 Modelled and observed change in groundwater level at well 160691_A

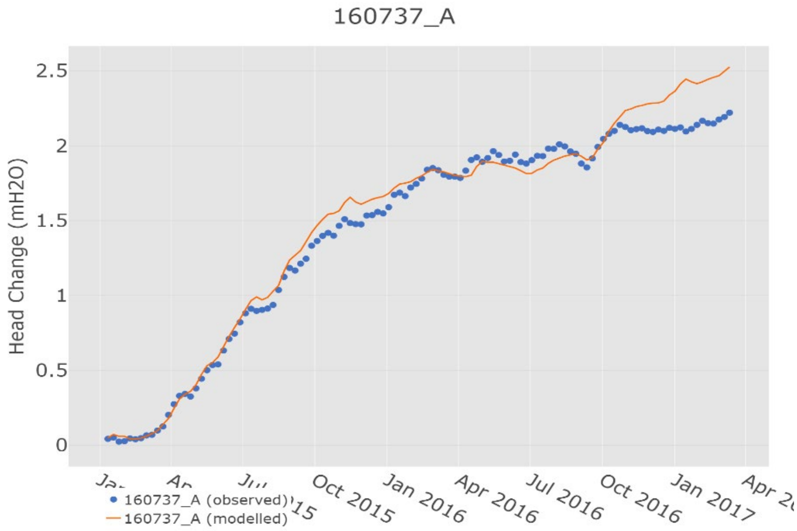

Figure S21 Modelled and observed change in groundwater level at well 160737_A

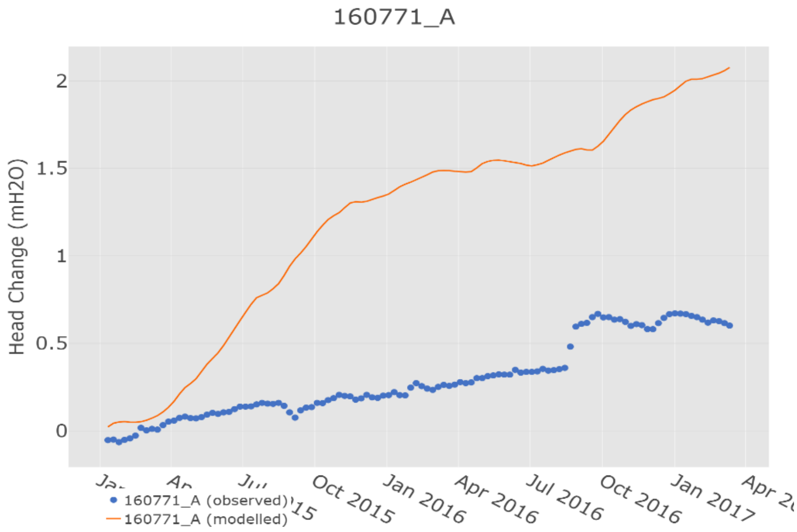

Figure S22 Modelled and observed change in groundwater level at well 160771_A

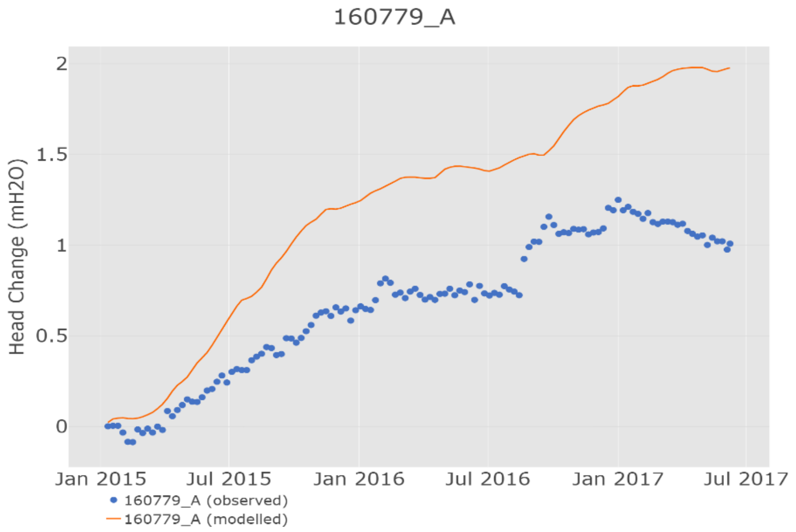

Figure S23 Modelled and observed change in groundwater level at well 160779_A

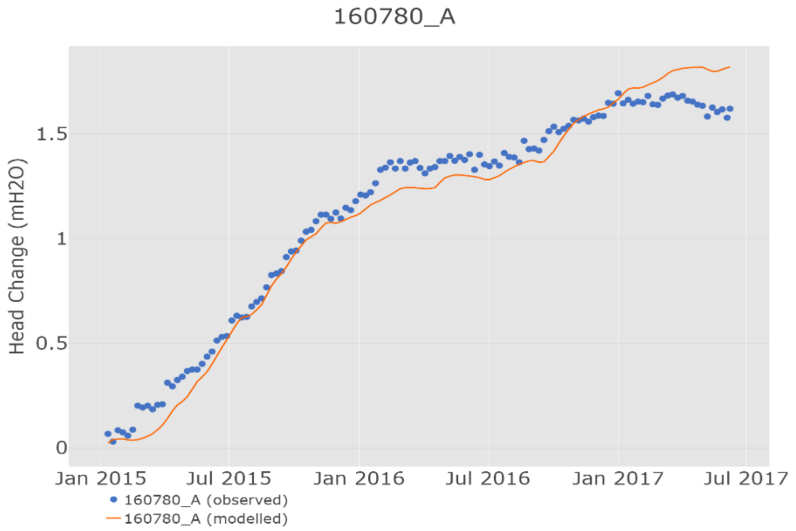

Figure S24 Modelled and observed change in groundwater level at well 160780_A

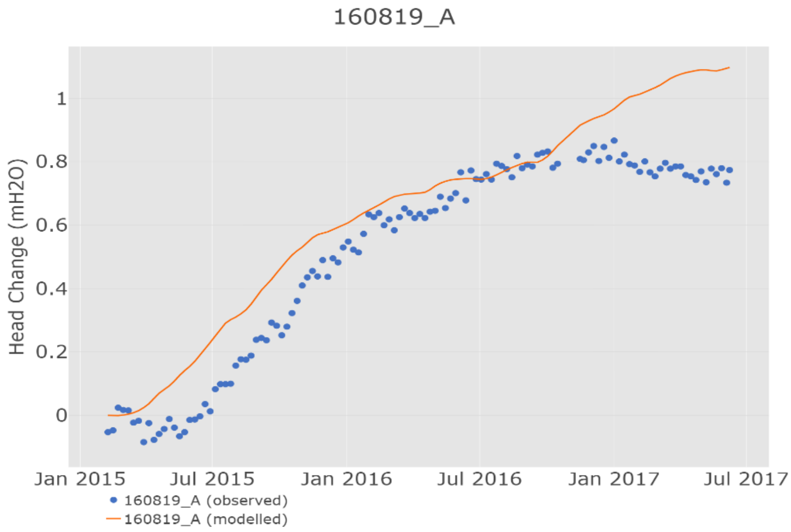

Figure S25 Modelled and observed change in groundwater level at well 160819_A

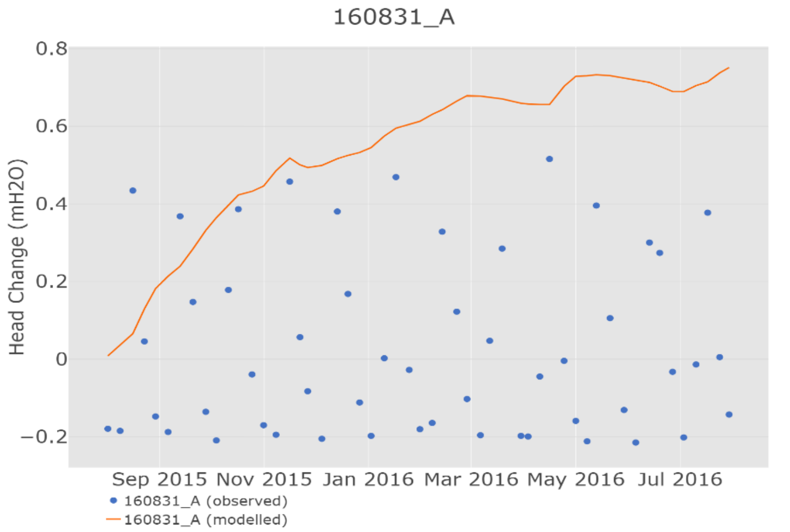

Figure S26 Modelled and observed change in groundwater level at well 160831_A

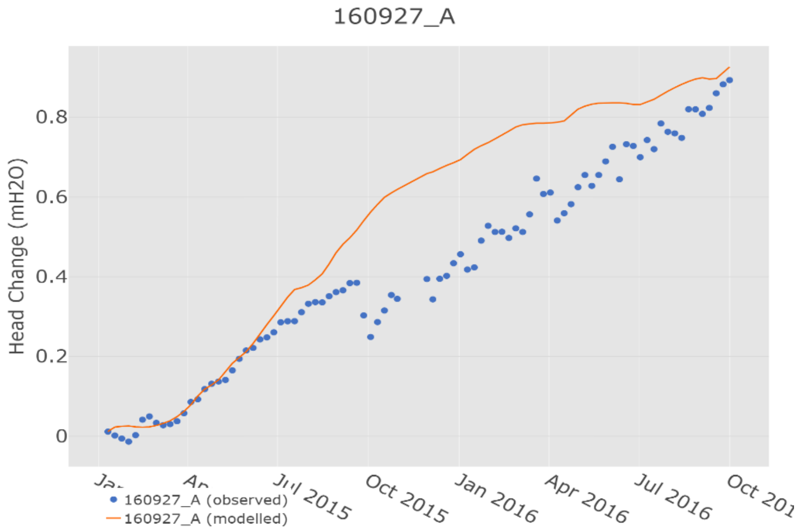

Figure S27 Modelled and observed change in groundwater level at well 160927_A

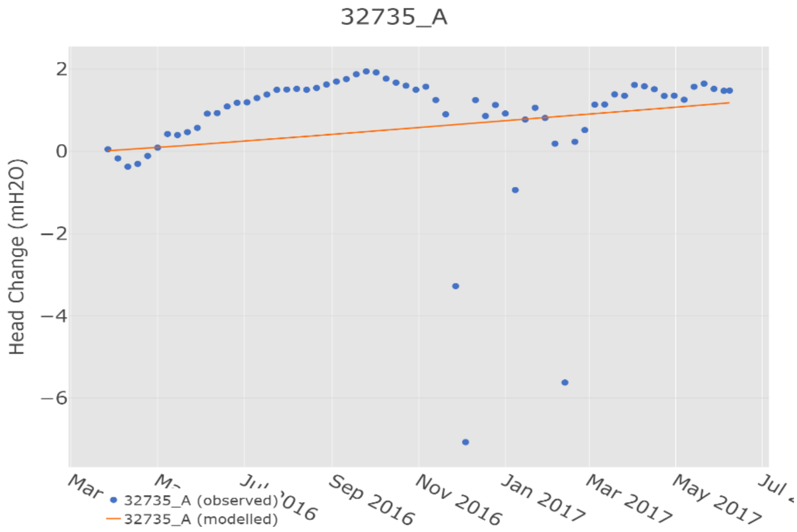

Figure S28 Modelled and observed change in groundwater level at well 32735_A

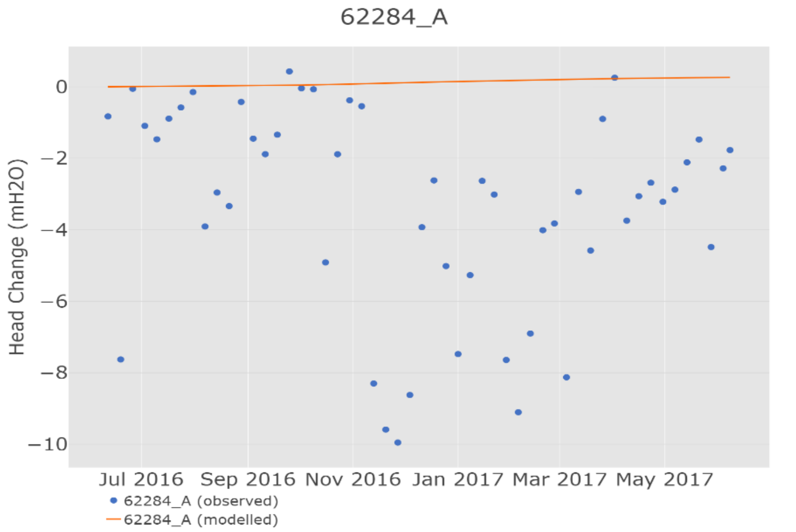

Figure S29 Modelled and observed change in groundwater level at well 62284_A

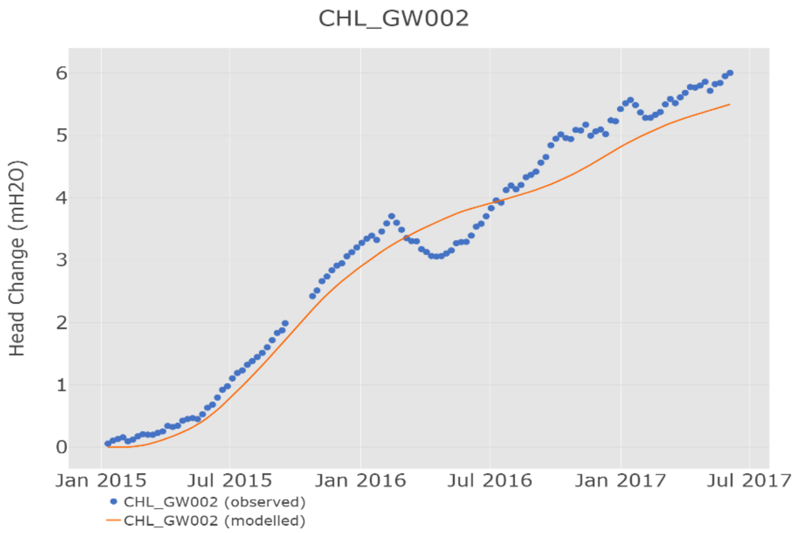

Figure S30 Modelled and observed change in groundwater level at well CHL_GW002

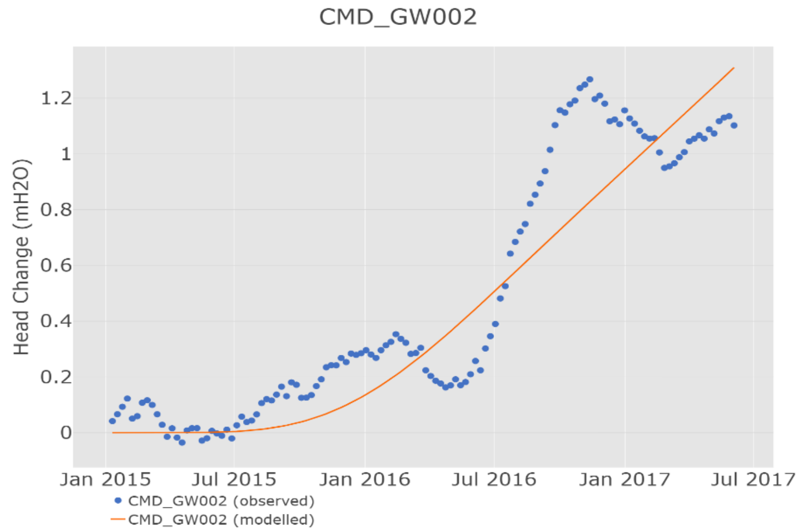

Figure S31 Modelled and observed change in groundwater level at well CMD_GW002

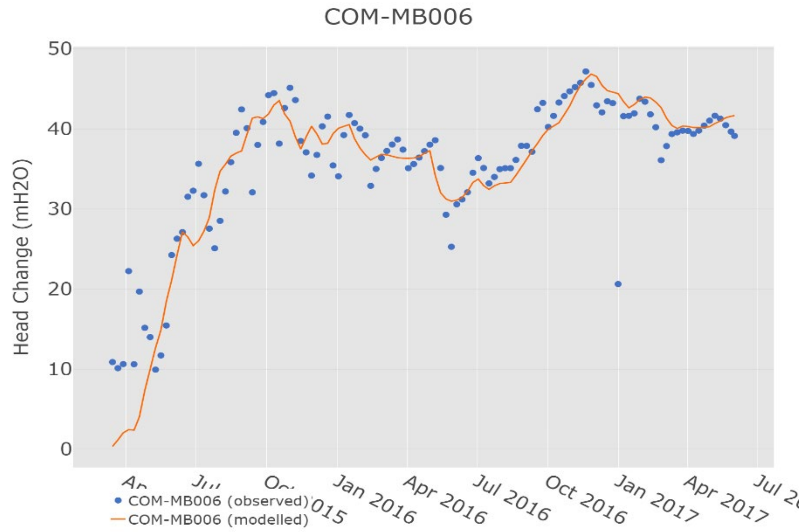

Figure S32 Modelled and observed change in groundwater level at well COM-MB006

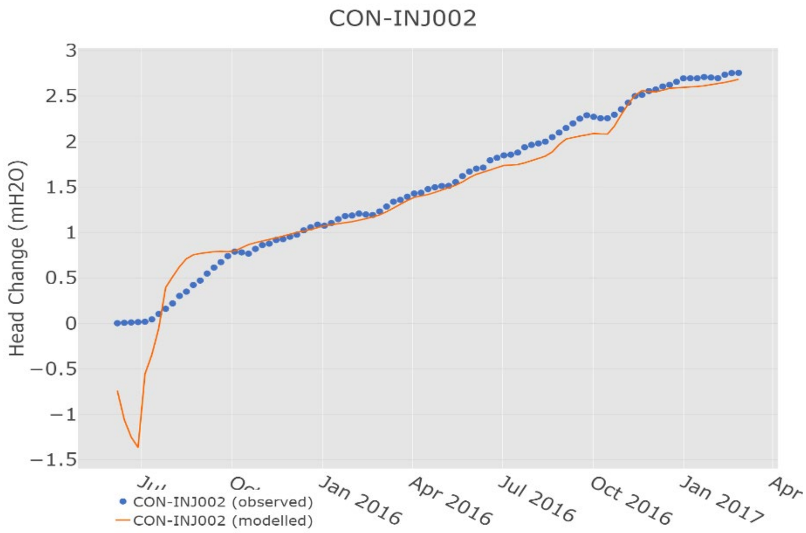

Figure S33 Modelled and observed change in groundwater level at well CON-INJ002

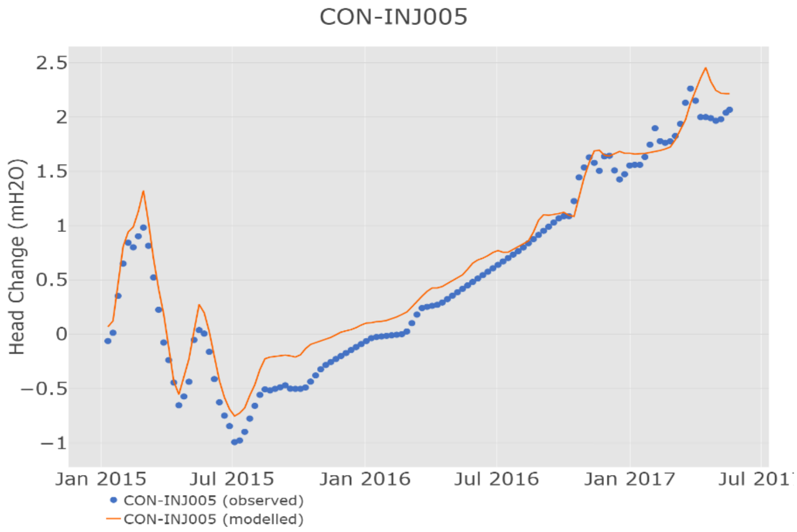

Figure S34 Modelled and observed change in groundwater level at well CON-INJ005

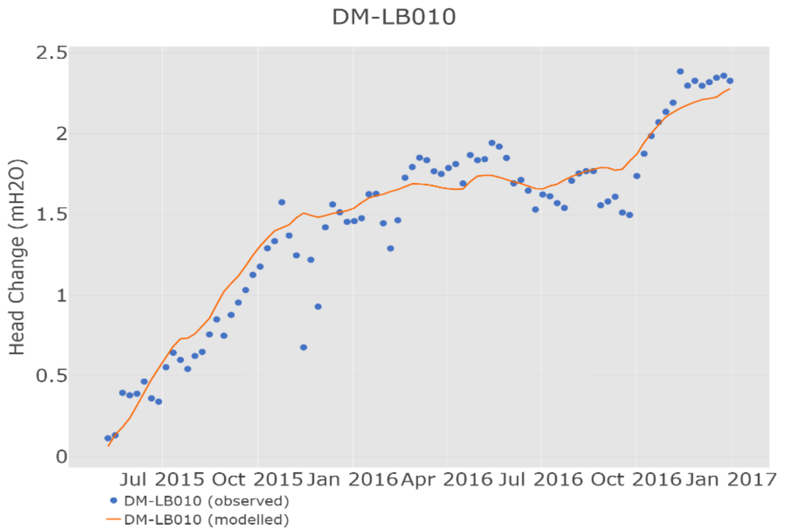

Figure S35 Modelled and observed change in groundwater level at well DM-LB010

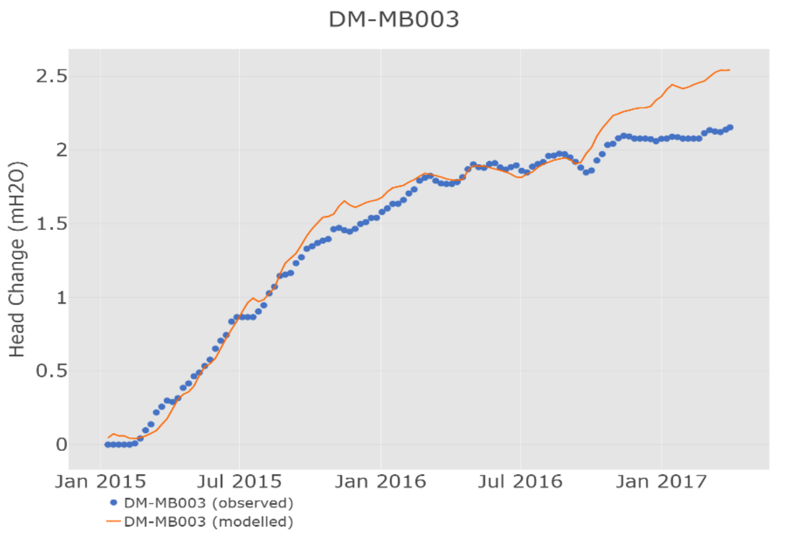

Figure S36 Modelled and observed change in groundwater level at well DM-MB003

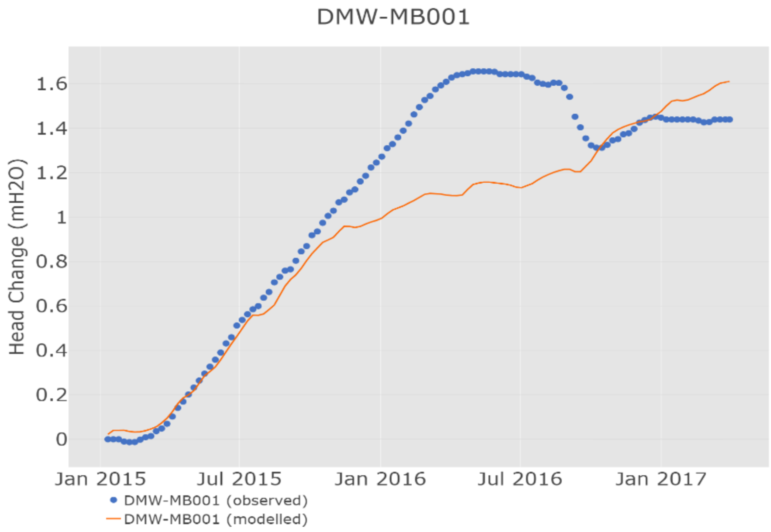

Figure S37 Modelled and observed change in groundwater level at well DMW-MB001

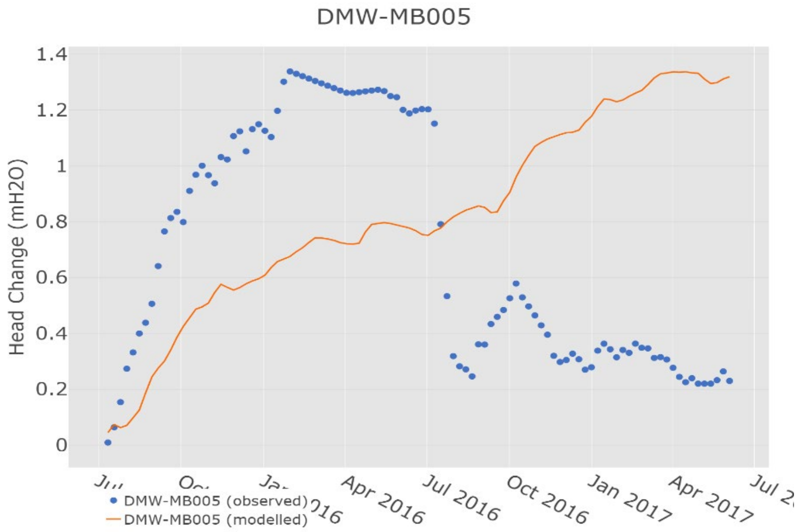

Figure S38 Modelled and observed change in groundwater level at well DMW-MB005

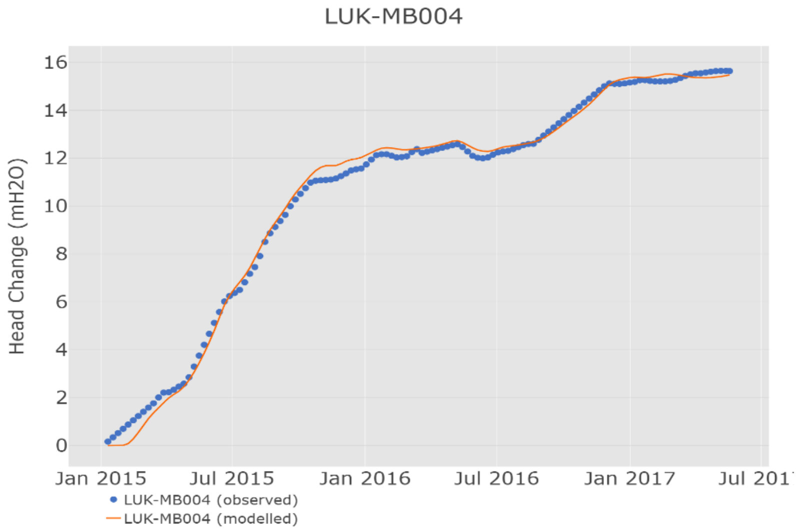

Figure S39 Modelled and observed change in groundwater level at well LUK-MB004

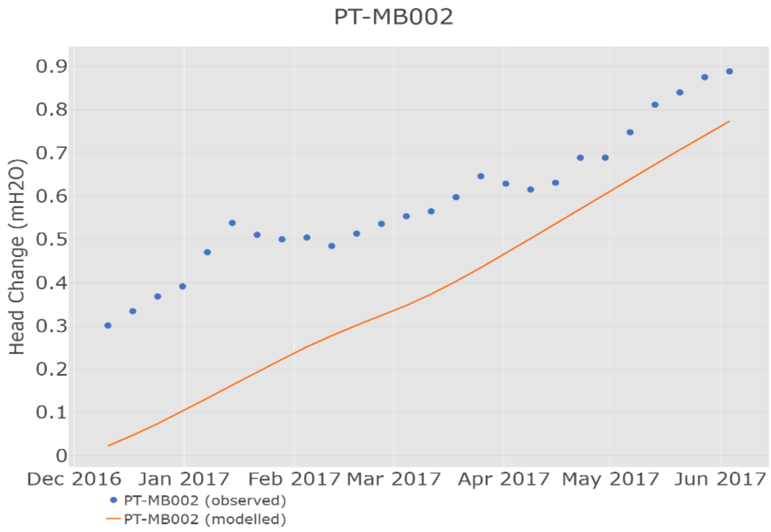

Figure S40 Modelled and observed change in groundwater level at well PT-MB002

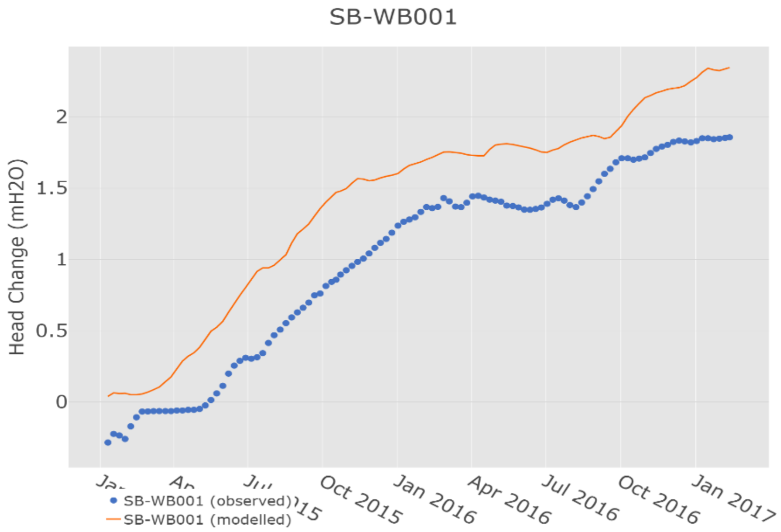

Figure S41 Modelled and observed change in groundwater level at well SB-WB001

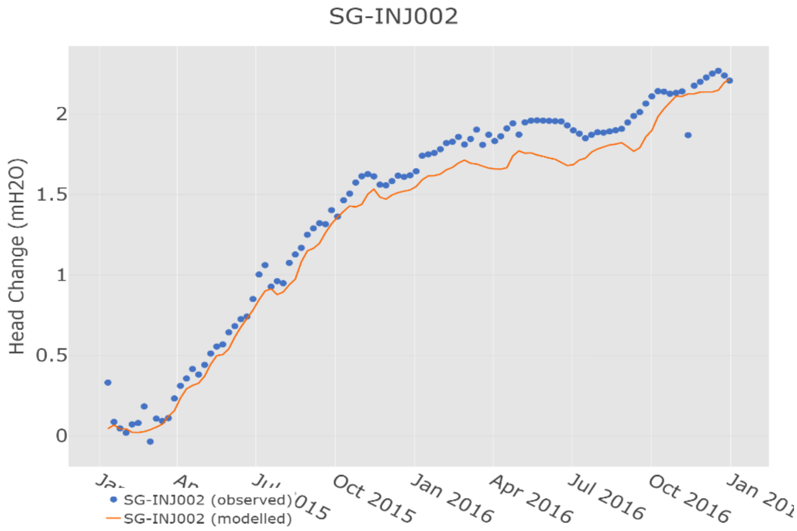

Figure S42 Modelled and observed change in groundwater level at well SG-INJ002

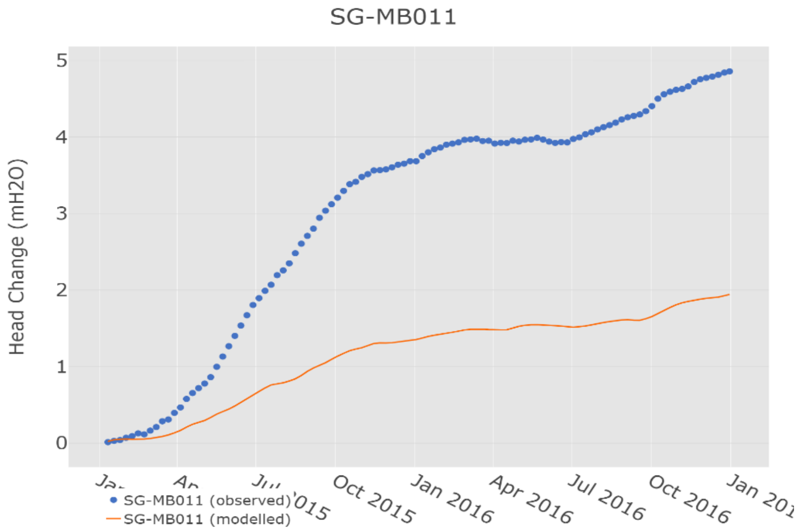

Figure S43 Modelled and observed change in groundwater level at well SG-MB011

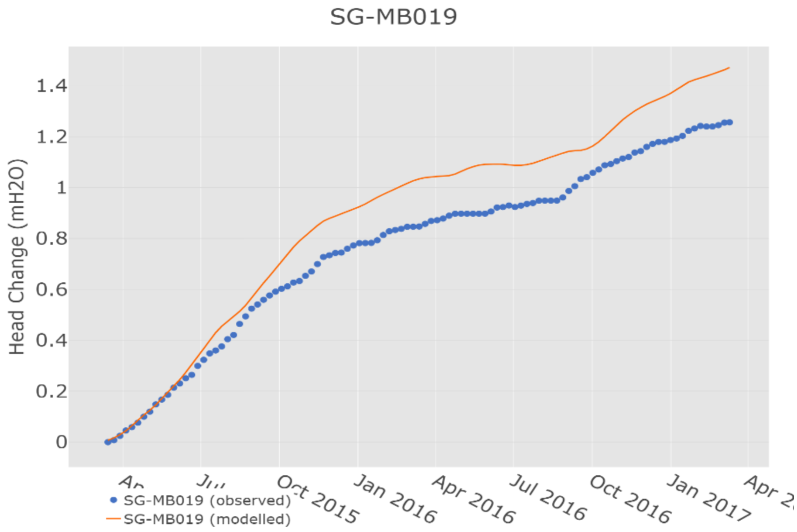

Figure S44 Modelled and observed change in groundwater level at well SG-MB019

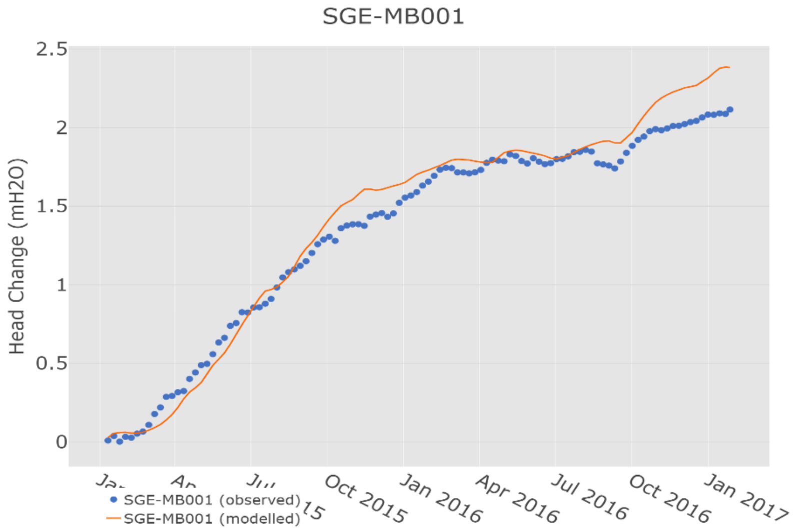

Figure S45 Modelled and observed change in groundwater level at well SGE-MB001

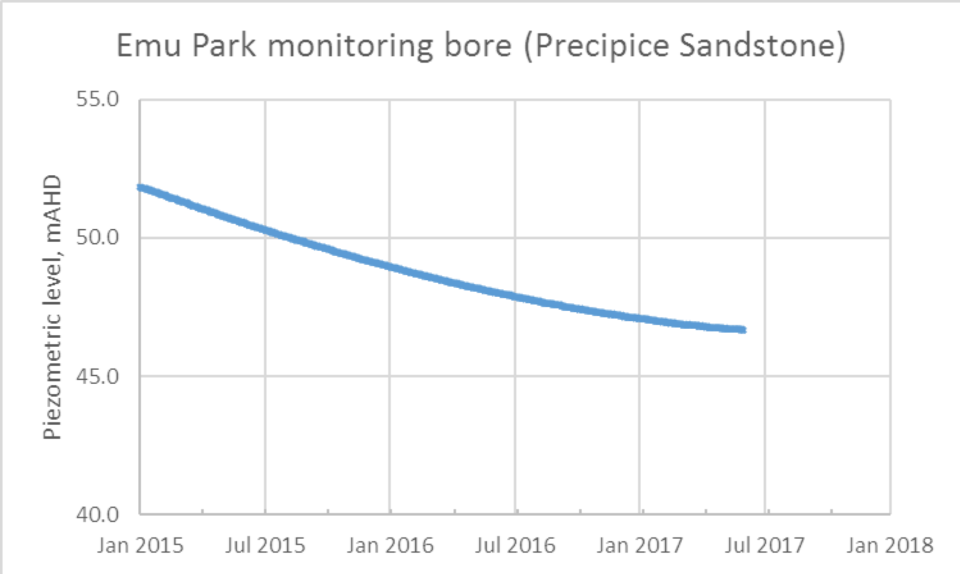

Figure S46 Observed change in groundwater level at the Emu Park bore demonstrating no response to MAR injection

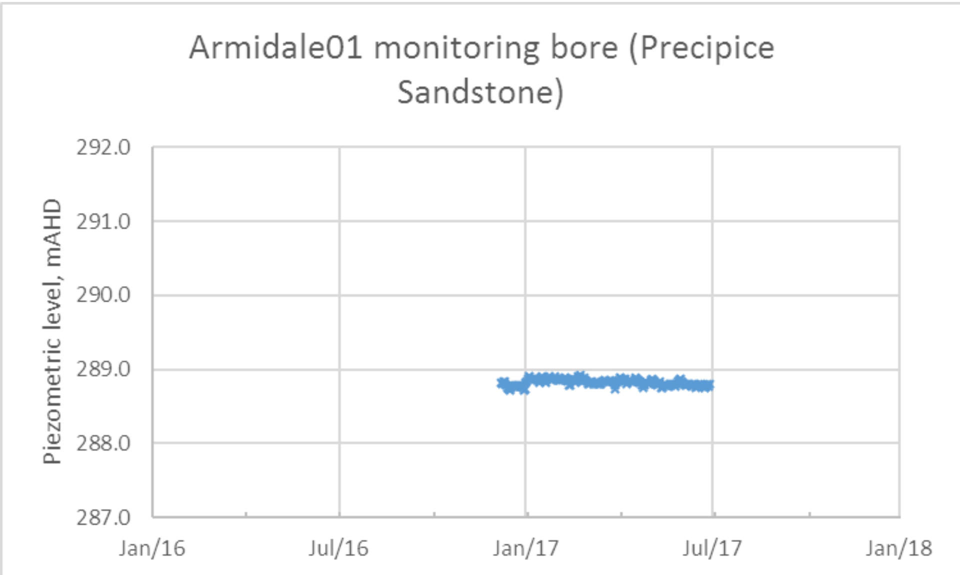

Figure S47 Observed change in groundwater level at the Armidale01 bore demonstrating no response to MAR injection